the abreviation Bi2201 is more conventional.

Chapter 5

Hall measurements on $BSCO_{2201}$

Low temperature Hall measurements are presented on $BSCO_{2201}$ over a wide doping range spanning the slightly underdoped to the far overdoped. A novel doping assignment scheme based on new Tl_{2201} data is trialled and was found to give reasonable dopings for $BSCO_{2201}$. The Hall data at low temperature shows possible linear behaviour at low temperature and interesting evolution of the low T Hall parameters which place constraints on an expected low temperature anisotropic term in either the scattering or the carrier density.

5.1 Sample growth

The samples were grown ~~and initially characterised~~ by Prof. Takeuchi's group in Sendai University, Japan in May 2009 using the floating zone technique. Here powders of the correct stoichiometry are compacted into a rod and fed slowly through a furnace where it becomes a viscous melt. The melt solidifies epitaxially on a seed crystal with impurities held in the melt portion of the crystal which gradually moves up, along the rod until it reaches the end of the rod and the growth is over. The end portion, containing the impurities is then removed. Similar samples have ~~already~~ previously been ~~extensively~~ studied ~~through~~ using ARPES and STM by members of the Sendai group [13, 86].

The point is that the molten zone travels along the crystal as it's grown.

Table 5.1 lists the nominal stoichiometries ~~for~~ of the sample ~~growth~~ grown as well as the annealing conditions. Also listed are the *nominal* T_c values for the source crystals which are used ~~in the naming~~ to name the samples. The actual measured T_c values of individual samples for the purposes of doping determination are slightly different due to different definitions of T_c*.

The samples are named according the convention,

B<Tc>K<Region><Crystal No.><Sample No.>

*The source crystals were defined based on the zero value T_c , the T_c for doping purposes is defined as the mid-point of the transition with an error based on the difference between the mid-point and the zero-point.

what does this mean.

Table 5.1: Growth details for the $BSCO_{2201}$ samples. OD, OP and UD stand for over, optimally and under doped respectively. T_c values are nominal.

Nominal composition								
Bi	Pb	Sr	La	Cu	O	T_c	Reg.	Annealing conditions
1.72	0.38	1.85	0.0	1.0	6+d	<2	OD	400 °C, 96 h in 2.5 atm. O_2
1.72	0.38	1.85	0.0	1.0	6+d	7	OD	750 °C, 24 h in air
1.72	0.38	1.85	0.0	1.0	6+d	16	OD	550 °C, 72 h in flowing N_2
1.35	0.85	1.47	0.38	1.0	6+d	30	OD	As grown
1.35	0.85	1.47	0.38	1.0	6+d	32	OP	650 °C, 72 h in flowing N_2
1.2	0.90	1.30	0.55	1.0	6+d	30	UD	As grown
1.2	0.90	1.30	0.55	1.0	6+d	28	UD	650 °C, 72 h in flowing N_2

so for example 'B00KOD2A' refers to the sample 'A' taken from the crystal 'B00KOD2' — the second overdoped crystal with a T_c of 0 K.

5.2 Size determination

Thicknesses were determined for some of the samples using the FIB or the optical microscope as described in the methods section. The thicknesses used to calculate absolute values of R_H are listed in table 5.2 and are marked in grey. FIB results are given for areas as close to the two voltage contacts that were visible in the scans. As can be seen in the example scan shown in figure 5.2.1, there is some variation in the depth along the sample length. Measurements are therefore taken as close to the voltage legs as possible and where appropriate suitable errors are estimated. — why?

The two scans shown are of good quality, however for the purpose of estimating errors in the thickness some of the scans presented problems. Samples B26KOD1A, B28KUD3A, B30KOD2 and B30KUD3 were obscured with the grease applied as part of the pulsed field measurements. Other samples were not correctly earthed such as B28KUD3B which made the images dark, whilst samples B07KOD2 and B32KOP3 were very flaky under close scrutiny. A scan of B30KOD3 showed that it was partially split in the ab plane which may contribute to systematic error in thickness estimate. In all these cases, the estimate in the thickness error was adjusted accordingly to compensate. A more comprehensive set of FIB scans, including images of the split in the layers can be found in Appendix C.

Figure 5.2.1: Top shows an image composited from several FIB scans along the length of sample B00KOD1A, with bottom right showing a detail of the right voltage leg. Bottom left shows an oblique top down view of sample B30KOD3.

The oblique view of B30KOD3 in figure 5.2.1 shows a clear misalignment of the voltage legs to the right of the image. This illustrates why it is necessary to take both positive and negative field sweeps in order to separate the magnetoresistance from the Hall components. This also explains why the length and width determinations were subject to large errors which affects the absolute value of the in-plane resistivity calculations.

5.3 Doping determination

Figure 5.3.1 shows measurements of the in-plane resistivity, $\rho(T)$, of the samples in zero field taken in the VTI in the Polo magnet. The mid-transition T_c values were extracted from the plots with the error determined from the difference between the mid point and the zero resistance point. Results are listed in table 5.3 as well as the normalised T_c values, $T_c/T_c(\mathrm{max})$, with $T_c(\mathrm{max}) = 36\,\mathrm{K}$. The derivatives of the same resistivity curves in figure 5.3.1 are plotted in figure 5.3.2 along with derivatives to temperature sweeps taken at 13 T. Here we can see in the overdoped samples the distinct slope downwards towards T_c which signifies the coherent quasiparticle

Table 5.2: Sample measurements as determined by optical microscope measurements and thickness as determined by FIB. Samples highlighted in grey were used for determining absolute values of R_H. A and B refer to each of the two contacts visible to the FIB scan. Measurements are in micrometres.

	Optical			FIB	
Sample	Length	Width	Thick.	Contact A	Contact B
B00KOD1A	781 ± 123	157 ± 49	N/A	45 ± 1	50 ± 5
B00KOD1B	627 ± 49	196 ± 44	39 ± 5	43 ± 1.5	45 ± 1.5
B07KOD1	1277 ± 74	392 ± 49	29 ± 10	N/A	N/A
B07KOD2	1061 ± 69	333 ± 74	N/A	20 ± 5	30 ± 1
B16KOD1A	795 ± 34	299 ± 34	N/A	24 ± 1	24 ± 1
B16KOD2A	358 ± 29	172 ± 54	9 ± 1	N/A	N/A
B16KOD3	1122 ± 44	368 ± 83	N/A	25 ± 2	24 ± 2
B30KOD1	436 ± 34	250 ± 44	21 ± 2	N/A	N/A
B30KOD2	344 ± 44	137 ± 29	20 ± 5	15 ± 4	15 ± 4
B30KOD3	255 ± 49	98 ± 25	N/A	16.5 ± 1.5	19 ± 1
B32KOP1	658 ± 83	397 ± 34	N/A	6.5 ± 1.5	6.5 ± 1.5
B32KOP2	441 ± 25	226 ± 20	10 ± 1	N/A	N/A
B32KOP3	437 ± 34	118 ± 20	N/A	6 ± 1	6 ± 1
B32KOP4	427 ± 74	137 ± 39	N/A	9 ± 3	9 ± 3
B30KUD1A	622 ± 49	447 ± 25	36 ± 3	N/A	N/A
B30KUD1B	828 ± 34	471 ± 64	35 ± 3	N/A	N/A
B30KUD2	545 ± 69	152 ± 39	N/A	5 ± 1	5 ± 1
B30KUD3	476 ± 49	118 ± 34	N/A	7 ± 2	7 ± 2
B28KUD2A	657 ± 29	250 ± 39	11 ± 1	N/A	N/A
B28KUD3A	633 ± 49	142 ± 34	N/A	16 ± 3	16 ± 3
B28KUD3B	653 ± 44	216 ± 49	N/A	16 ± 3	16 ± 3

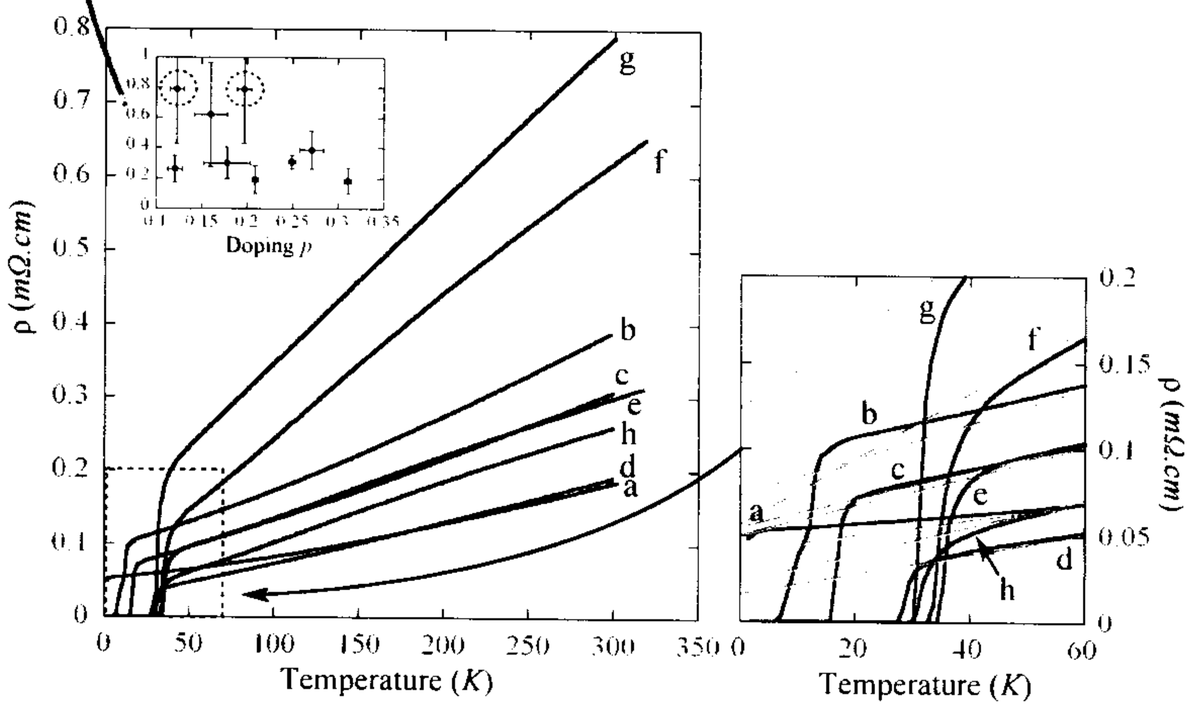

Figure 5.3.1: The in-plane resistivity measured in zero field. From nominally overdoped to underdoped, samples are (a) B00KOD1A, (b) B07KOD2, (c) B16KOD1A, (d) B30KOD3, (e) B32KOP1, (f) B32KOP4, (g) B30KUD3, (h) B28KUD3A. Right panel shows a zoomed portion of the curves at the transition temperatures along with continuations of fits to portion of the curve above T_c in red. Inset shows $\rho(300\,\mathrm{K})$ vs. doping with errors due to size determination.

region which begins at T_{coh}. This gradually levels out as doping is reduced until we observe a kink which marks the pseudogap temperature, T^*. The T^* kink is weaker in B30KUD3 than the optimally doped samples and in fact only appears, at a much lower temperature, when the field is applied. This suggests that it is in fact more doped than the optimally doped samples rather than less doped as the nominal composition would suggest. If we consider B30KUD3 to be overdoped rather than underdoped then this trend continues right across the range of samples.

Figure 5.3.3 shows the dopings as determined by the three different methods outlined in the experimental methods chapter. The dopings of the crystals range for $p = 0.12$ to $p = 0.31$ hole per Cu atom with significant discrepancies between the methods. The Ando determination bunches the doping values around a much narrower range, whereas the dopings determined by comparing with the Tl_{2201} dHvA data, spread the overdoped values over a wider range. The Tallon method sits between the two.

Figure 5.3.4 present Hall data at 300 K again taken in the Polo with comparable data from Konstantinović *et al.* [92]. It is clear that the Ando assignment of dopings is too confined with the data not at all following the

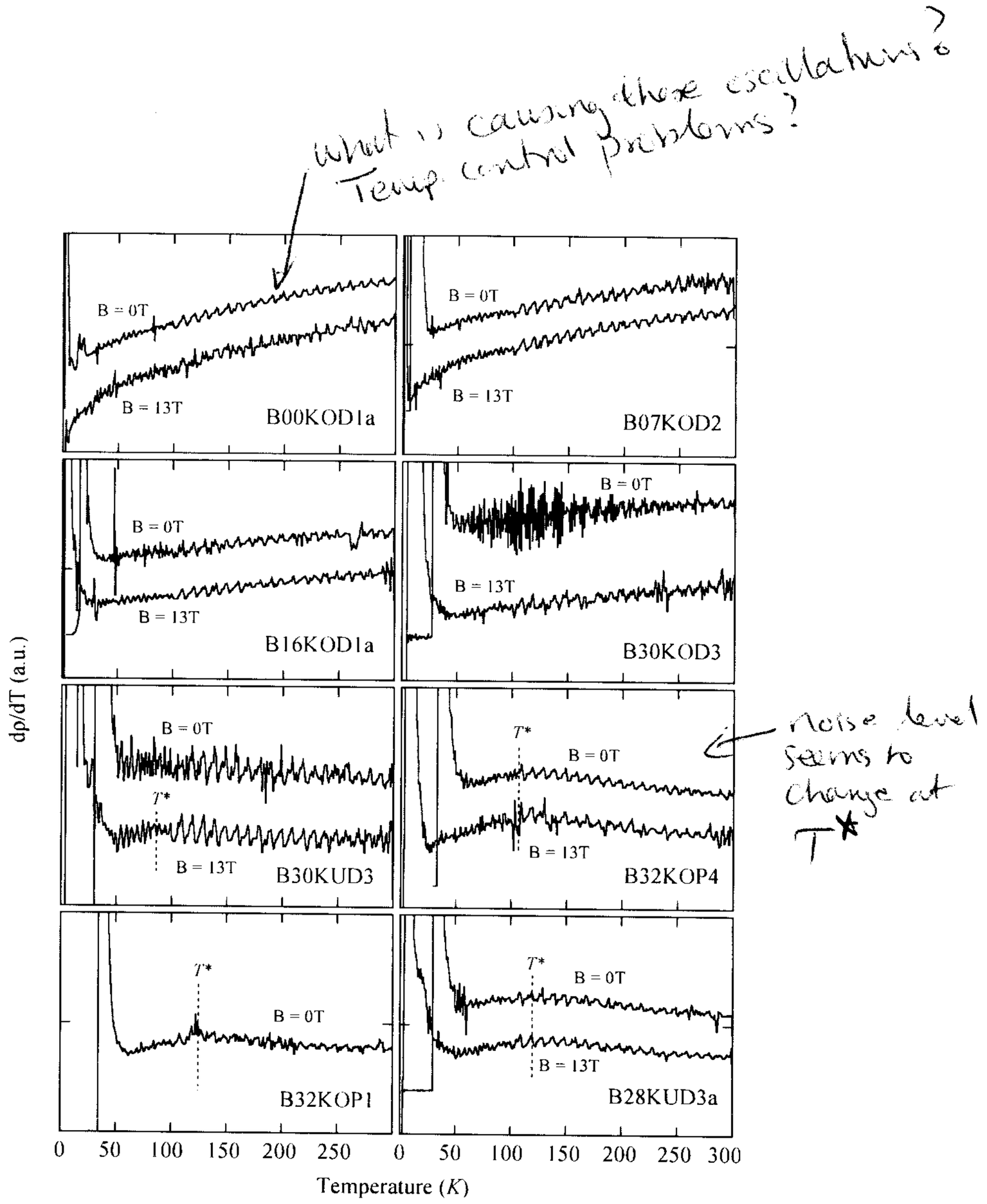

Figure 5.3.2: $d\rho(T)/dT$ curves for each of the samples taken in 0 T and 13 T field. Note the evolution of the $T_{\rm coh}$ gradient in the overdoped samples which give way to the T^* kink in the underdoped samples, B30KUD3 has been repositioned to follow this trend.

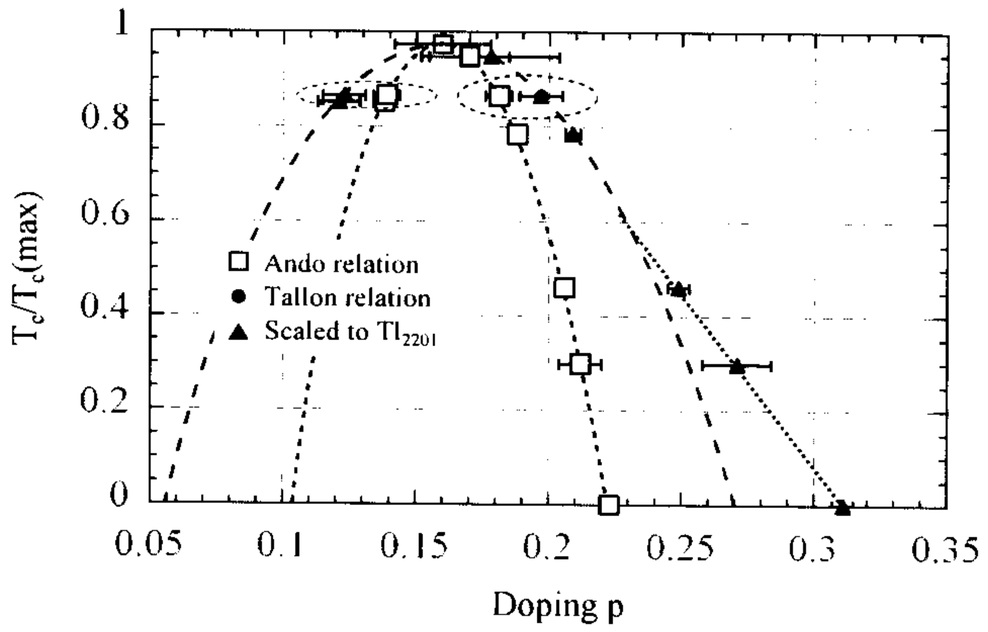

Figure 5.3.3: Doping distributions for the three different methods. From left to right, B28KUD3A, B30KUD3 (Assume UD), B32KOP1, B32KOP4, B30KUD3 (Assume OD), B30KOD3, B16KOD1A, B07KOD2, B00KOD1A. Broken lines are a guide to the eye. Circled points are B30KUD3 for both the overdoped and underdoped scenarios.

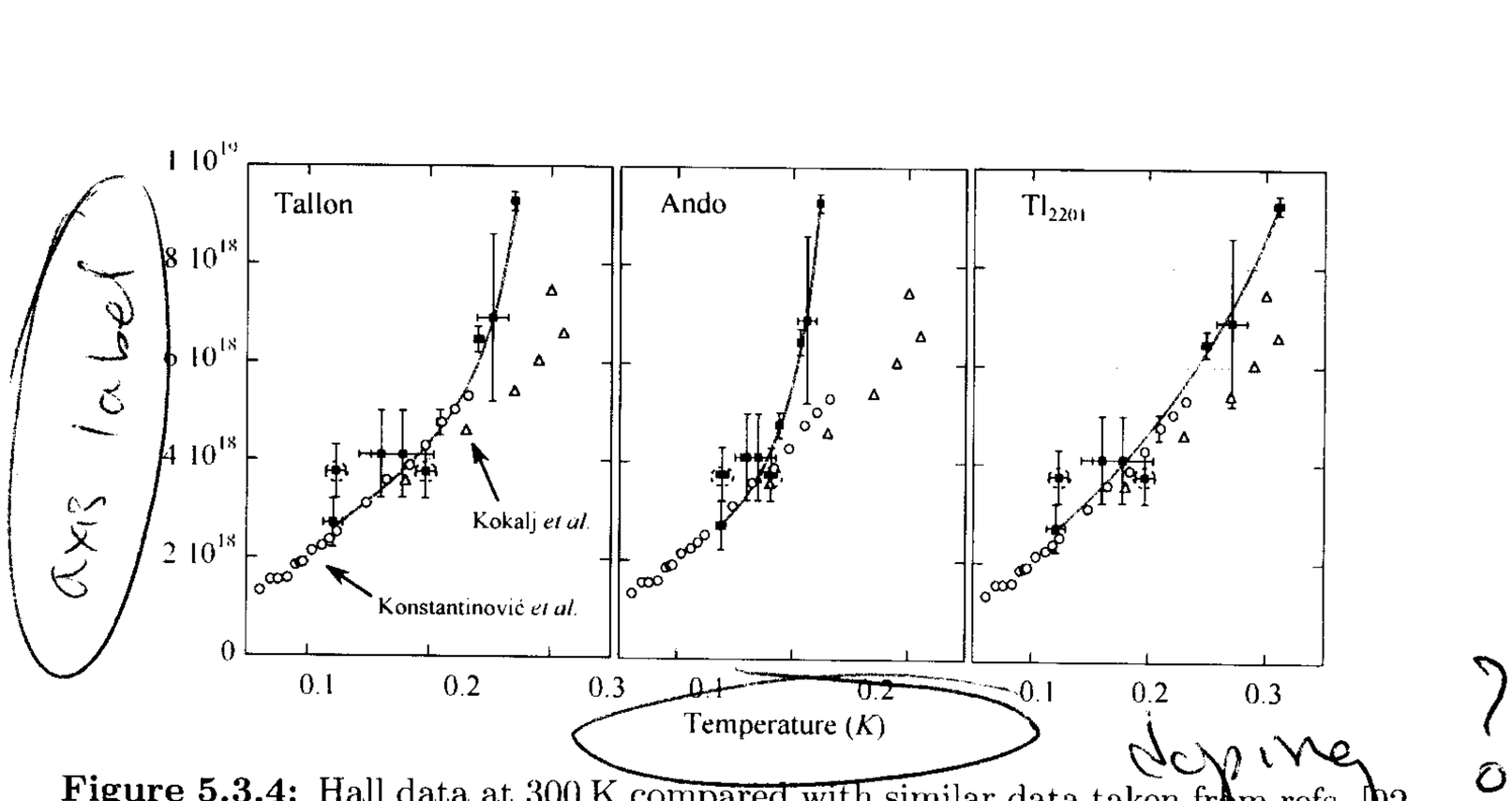

Figure 5.3.4: Hall data at 300 K compared with similar data taken from refs. [92, 93] using different doping assignments. From left: Tallon relation, Ando relation and scaling to Tl_{2201} data. Red lines are guides to the eye, circled points are B30KUD3 in the overdoped and underdoped positions.

respective curves whereas the Tallon relation follows much close the shape of the curve, although, perhaps this is not surprising given that the dopings in the Konstantinovoć paper were also assigned using the Tallon relation. However what is most interesting is that when compared with Tl_{2201} data from Kokalj *et al.* [93] which we know is appropriate to scale to the Tl_{2201} doping scheme, we see that of the three methods, scaling the $BSCO_{2201}$ to the Tl_{2201} dHvA data matches the closest. On this rationale, we continue assuming that the Tl_{2201} doping assignments are the correct ones.

Also, referring to the circled points, we see that again the data is more consistent if we consider the B30KUD3 to be overdoped rather than underdoped. Looking back to the inset of figure 5.3.1 we see that there is large scatter in the data points due to uncertainty in the dimensions which were determined by optical microscope, however there is an approximate downward trend with doping which is similar to what is found in the literature [9, 10, 92, 94]. Although B30KUD3 is more consistent to this trend in the underdoped position, the trend still lies with the error bars of the overdoped position. Looking ahead to the inset of figure 5.5.4 which shows R_H values at 300 K vs. doping, which depend only on the measurement of depth — which was much more accurately determined by the FIB — we see that the underdoped position lies far outside the overall trend even when considering the error bars.

5.4 Temperature sweeps

Figure 5.3.1 shows the in-plane resistivity, $\rho(T)$ for each of the samples in zero field taken in the VTI in the Polo magnet. From this plot we can characterise the T_c of the samples and find the residual resistivity, ρ_0 by using simple linear fits to the data above the transition temperatures and extrapolate back to zero. Table 5.3 show the fit parameters for each of the samples. The residual resistivities are very good with only one being above 100 μΩcm and most below 70 μΩcm which has been cited as being exceptionally good for $BSCO_{2201}$ [9]. Moreover the T_c of the optimally doped sample is 36 K which is amongst the highest reported [9] which again is testament to the crystal quality. ρ_0 generally increases as you move away from critical doping which lends support to the notion that La doping increasing the disorder in the CuO layers.

Table 5.3: Fits parameters to $\rho = \rho_0 + \rho_1 T$ for zero field resistivity data above T_c as well as T_c values determined from the same plots. Fits at low T are shown in inset to figure 5.3.1.

Sample	ρ_0(μΩcm)	ρ_1(μΩcm)	T_c (K)	T_c/T_c(max)
B00KOD1A	40.7	0.454	0 ± 1.0	0.00 ± 0.03
B07KOD2	73.0	1.026	11 ± 3.8	0.31 ± 0.11
B16KOD1A	49.9	0.843	17 ± 1.0	0.47 ± 0.03
B30KOD3	15.9	0.578	29 ± 0.5	0.81 ± 0.01
B32KOP1	54.2	0.824	36 ± 1.0	1.00 ± 0.03
B32KOP4	55.6	1.904	35 ± 2.0	0.97 ± 0.06
B30KUD3	123.0	2.233	32 ± 1.0	0.89 ± 0.03
B28KUD3A	22.6	0.806	32 ± 1.0	0.89 ± 0.03

The inset to figure 5.3.1 shows the $\rho(300\,\mathrm{K})$ values for the samples along with error bars due to uncertainty in the size determination. As we saw in the previous section, there is significant misalignment and overall width to the voltage contacts which lead to large systematic errors which affect scaling only. Nonetheless, there appears to be an downward trend in resistivity as doping is increased. The circled points are B30KUD3 in both the overdoped and underdoped position and although the position is perhaps more fitting in the underdoped position, there error bars leave the overdoped point well within the overall trend.

already said this and it is not true!

5.5 Hall plots

Figures 5.5.1, 5.5.2 and 5.5.3 show the Hall coefficients extracted as described in the methods section for samples progressing from overdoped, optimally doped to underdoped respectively. Where appropriate, the data is compared to that from Ando *et al.* [9]. Red lines in the plots are guides to the eye.

For the samples of $T_C >= 28$ K there are some data ~~which did not reach~~ where there was sufficient field to obtain linear behaviour versus (B) which are circled with a dashed line in the plots. For sample B30KOD2, many of the sweeps for $T < 45$ K showed significant hysteresis due to temperature drift. Despite temperature correction, many of the fits did not pass through the origin (circled in the figure) which is a good indicator that the true field suppressed linear Hall has

show plots of this

which figure

not been obtained. The same goes for the circled points on the B30KUD2 plot and another data point at $T = 1.5\,\mathrm{K}$ and $R_H = 7.3 \times 10^{-3}\,\mathrm{cm}^3$ from the first trip to LNCMI which is outside the plot boundary as well as data points on the plot for B28KUD3B. The data sets are combined, minus the points highlighted in the previous paragraph, in the main panels of figure 5.5.4 alongside the data from the Ando paper.

With reference to figure 5.5.4 and in particular the new low temperature data points, we see that doping strongly affects the qualitative shape of the R_H curves. Whilst the trend appears to be that $R_H(300\,\mathrm{K})$ decreases as doping increases as to be expected, the $R_H(0\,\mathrm{K})$ values all tend toward approximately similar values of around $0.5 \times 10^{-3}\,\mathrm{cm}^3$ to $1.5 \times 10^{-3}\,\mathrm{cm}^3$. The most pronounced difference between high and low temperature values though is with the optimally doped samples which are around $\times 2.75$ greater at high temperature. Right down to 0 K there is no sign change in R_H, which suggests that the hole pockets have higher mobility than the electron pockets across the range of dopings studied.

The error bars on the data points do not include error from the thicknesses which are systematic across the data points. The inset of figure 5.5.4 shows the R_H values at 300 K vs. doping for each of the samples with these error bars applied. The overall trend is downward with doping with the progression being approximately monotonic, however the exception is B16KOD1A which has a slightly lower R_H than would be expected from a linear trend.

The Hall angle is plotted for each of the samples where $B = 0\,\mathrm{T}$ in-plane resistivity data is available in figure 5.5.5 with temperature raised to a fitted exponent, α. In the original Chien analysis, $\alpha = 2$ but is allowed to vary here to observe deviations from the expected T^2 behaviour. Similar analysis was performed for resistivity data taken at $B = 13\,\mathrm{K}$ and although these plots are not shown, the fitted α values are plotted in the bottom left subplot along with the $B = 0\,\mathrm{T}$ values. A nominal unitary field was used when calculating $\cot\theta_H$ and only data above the superconducting transition was fitted and is shown in the plots. Note that for the $B = 13\,\mathrm{T}$ case, the Hall data for the optimally doped sample B32KOP1 was compared with resistivity data for sample B32KOP4 which explains the slightly different doping value assigned to it. In this particular instance, it appears that the assignment of the sample B30KUD3 would be more suited to underdoped

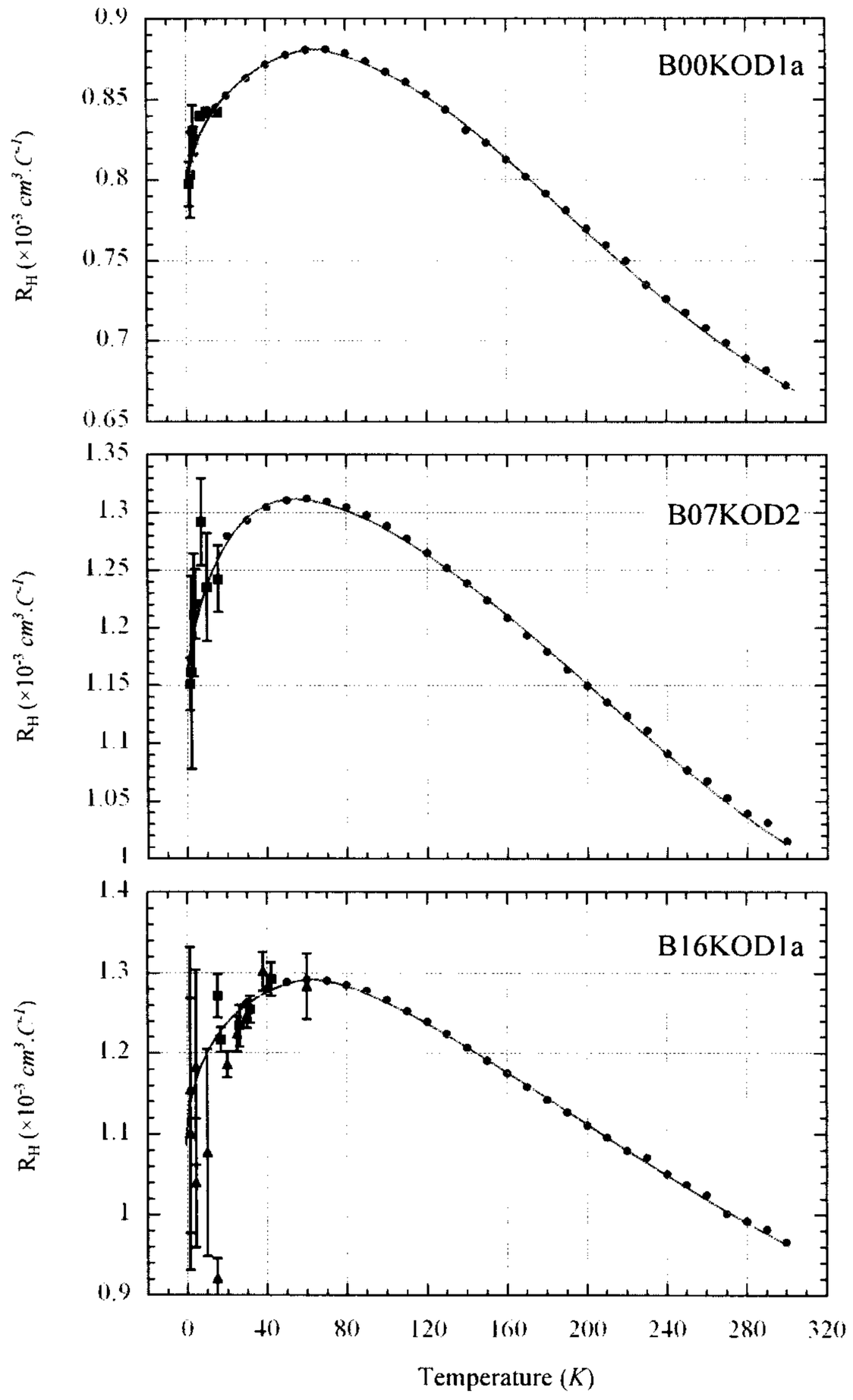

Figure 5.5.1: R_H for underdoped samples of $BSCO_{2201}$. Plots show results from, • Polo in June 2010, ▲ LNCMI in June 2009, ▼ LNCMI in Feb 2010, ■ Nijmegen in May 2010. Symbols for comparable samples are marked on the plots. Red lines are a guide to the eye.

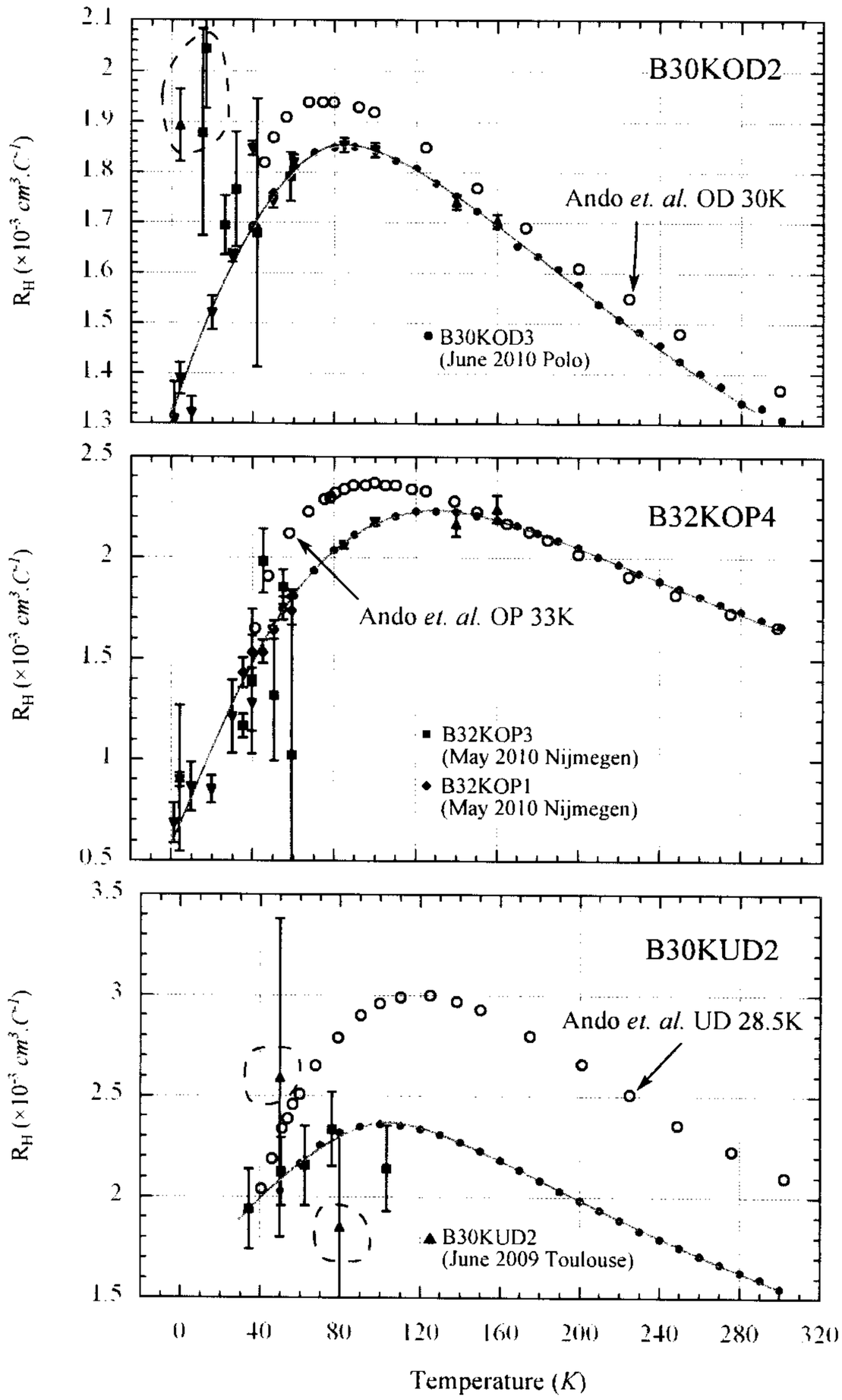

Figure 5.5.2: R_H for underdoped samples of $BSCO_{2201}$. Plots show results from, • Polo in June 2010, ▲ LNCMI in June 2009, ▼ LNCMI in Feb 2010, ■ Nijmegen in May 2010. Symbols for comparable samples are marked on the plots. Dashed lines indicate points where the field was not sufficient to achieve linear behaviour. Red lines are a guide to the eye.

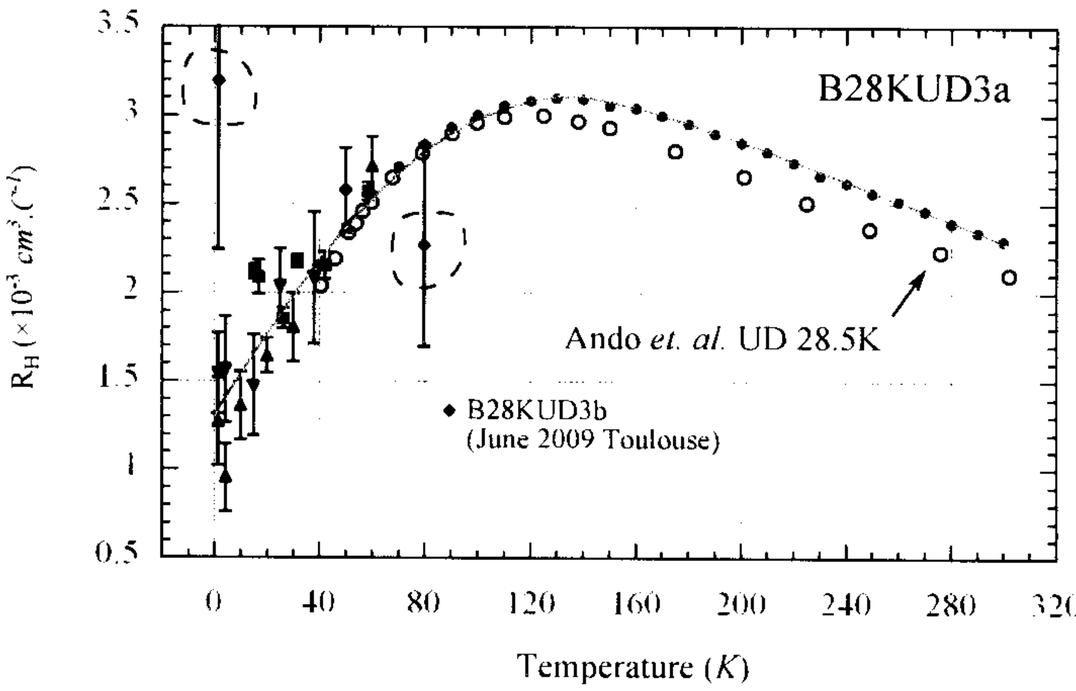

Figure 5.5.3: R_H for underdoped samples of $BSCO_{2201}$. Plots show results from, • Polo in June 2010, ▲ LNCMI in June 2009, ▼ LNCMI in Feb 2010, ■ Nijmegen in May 2010. Symbols for comparable samples are marked on the plots. Dashed lines indicate points where the field was not sufficient to achieve linear behaviour. Red lines are a guide to the eye.

rather than overdoped.

With reference to the plot in the lower left, the fitted exponents approximately follow the same downward trend with doping as in $BSCO_{2201}$ data from Konstantanović *et al.* [95] up to around $p = 0.27$. In particular the $B = 13$ T follows the curve reasonably closely before the upturn at $p = 0.31$. Downward deviation from the T^2 behaviour at high temperatures (as indicated from a drop in the α exponent) at this point in the phase diagram has been previously interpreted to be due to the saddle point in the DOS which is approaching from below the Fermi energy [96] which would also explain why there is a recovery toward T^2 behaviour between $p = 0.27$ and $p = 0.31$ as the flat portion of the DOS passes above the Fermi energy. This would suggest that the van-Hove singularity peaks in the $BSCO_{2201}$ phase diagram at around $p = 0.25$, approximately where the B16KOD1A sample lies and where the room temperature R_H value was also found to be slightly lower than expected. However this occurs at a higher doping than the Hashimoto paper would suggest [14] (see figure 1.1.6) and given the proximity of the van-Hove singularity, the low Hall coefficient should not be interpreted a simple indicator of carrier density.

An alternate explanation based on the Narduzzo paper [70] goes as fol-

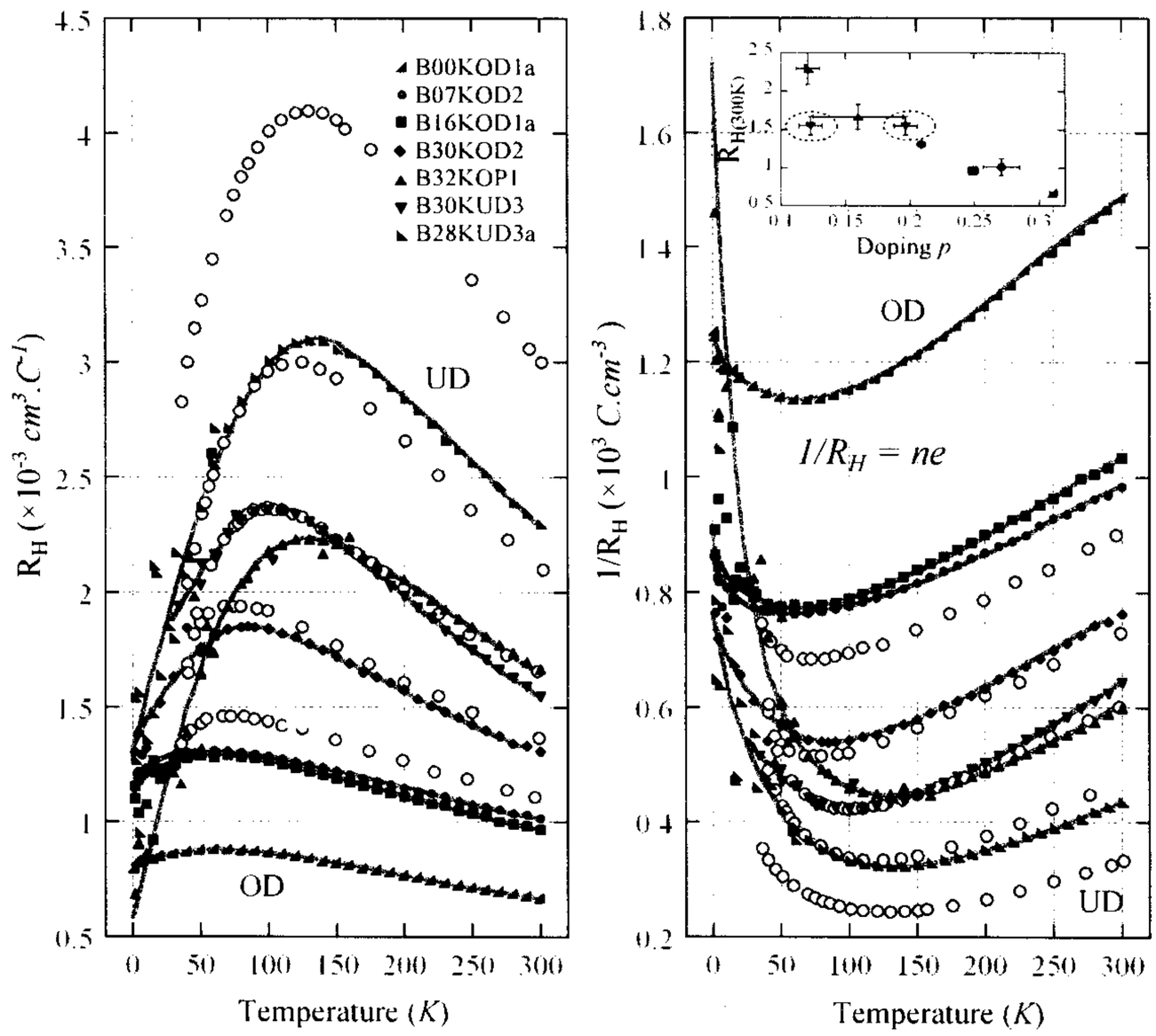

Figure 5.5.4: Hall data in context with data from Ando *et al.* [9] (open circles) which are in order of increasing R_H, 24KOD, 30KOD, 33KOP, 28.5KUD, 20KUD. Right panel shows the inverse hall data which relates to carrier density. Red lines are the same guides to the eye used in previous figures. Inset shows R_H at 300 K plus systematic error bars due primarily to uncertainty in thickness vs. doping scaled to Tl_{2201} data. B30KUD3 (circled) is plotted in both the overdoped and underdoped positions.

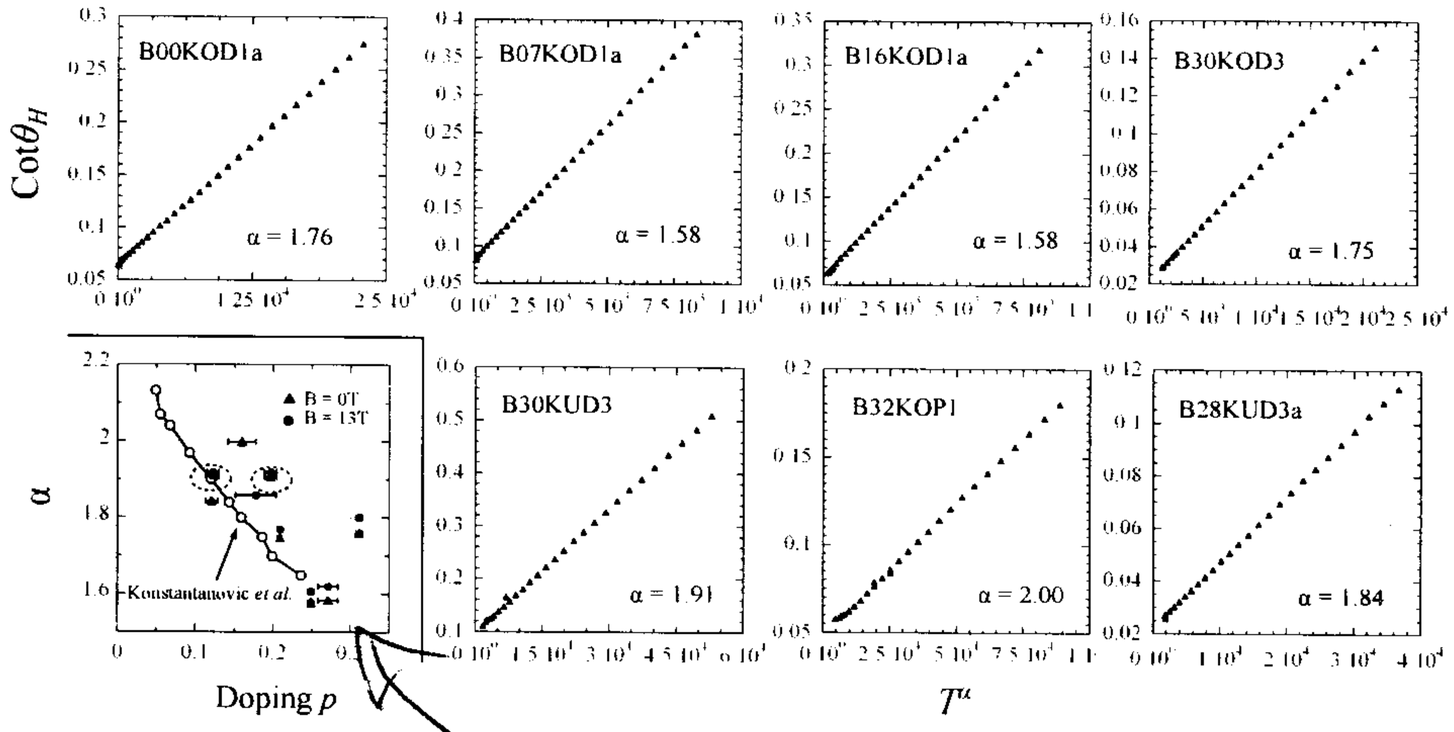

Figure 5.5.5: Hall angle calculated with a nominal field of unity from resistivity data taken in zero field. Plot in bottom left shows the fitted exponent, α, vs. doping compared with similar data on $BSCO_{2201}$ from Konstantanović *et al.* [95] for both zero field resistivity data and resistivity data taken at 13 K ($\cot\theta_H$ plots for $B = 13$ T not shown)

?

Surely you should be plotting α from the $\cot(\theta_H)$ plots vs doping not a fit to the resistivity — this makes no sense.

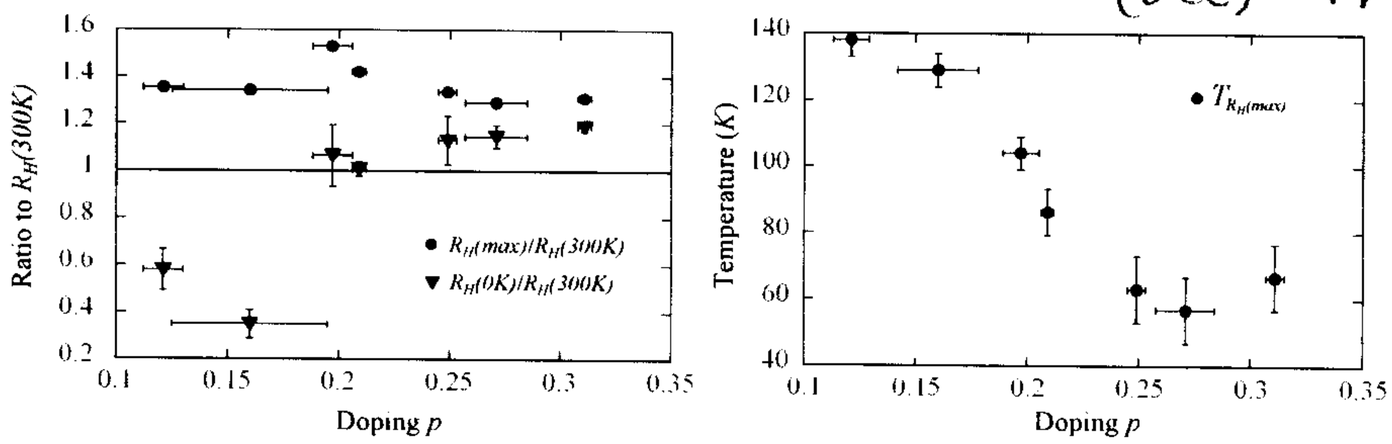

Figure 5.5.6: Left shows ratio of R_H values at the maximum of the Hall curves and at $T = 0$ K to the $T = 300$ K R_H values. Errors in R_H(0 K estimated from Hall plots, the value for B30KUD2 is estimated based on linear extrapolation. Right shows the temperature where the maximum R_H occurs.

lows. For $p \gtrsim 0.19$, $R_H(0\,\mathrm{K}) > R_H(300\,\mathrm{K})$ as illustrated in figure 5.5.6. If we assume there is not temperature dependent change of the Fermi surface such that would affect $\boldsymbol{v_F}$, then this can be explained by an temperature dependent change in scattering that preferentially affects one of the two regions of curvature (hole-like or electron-like) on the Fermi surface i.e. a change in anisotropic scattering. As detailed in the introduction, such scattering is thought to originate in the overdoped side of the phase diagram and is seemingly closely tied to superconductivity. The Narduzzo paper explores this possibility but ultimately could not definitively conclude that the scattering rate is proportional to $\cos^2(2\phi)$ as is the case in the Abdel-Jawad paper [97] detailed in the introduction.

To explain the anisotropy in the van-Hove scenario where the change is thought to come about from a change in the carrier numbers, we must surmise that the flat band does not lie at the same energy all around the Fermi surface in order to achieve this anisotropy — in effect this leads to a momentum dependent carrier term. This has been observed in cuprates with Platé *et al.* [76] demonstrating in Tl_{2201} a momentum dependence of the energy of the flat region of the bandstructure that range between -25 meV and -40 meV. However, along the (π, π) direction in this case, the van-Hove peak was suppressed suggesting that scattering too is anisotropic.

When we consider the ratio of the maximum R_H to the 300 K value also plotted in figure 5.5.6 then we see that these values do not vary much at all with doping indicating that the scattering process that suppresses the low temperature Hall values only becomes dominant below the temperature where $R_H(\mathrm{max})$ occurs. Moreover we note that the low temperature behaviour of R_H which, although not possible to ascertain for certain due to the scatter in points, appears linear in temperature below $R_H(\mathrm{max})$, which suggests that the same process explored above is T-linear in behaviour.

A finally observation is that when the temperatures of the maximums in R_H are plotted in figure 5.5.6, they show a similar doping behaviour to the α fitted exponents.

5.6 Conclusions

High quality crystals of Pb and Sr doped $BSCO_{2201}$ were sourced and studied in the normal state by magnetotransport measurements down to low tem-

peratures, thereby determining the low temperature Hall behaviour. We found evidence that determining the doping in $BSCO_{2201}$ by normalising to a hybrid combination of the Tallon relation for optimal and underdoped samples and to the Tl_{2201} data for overdoped samples gives dopings which are more consistent with the literature.

Two possible scenarios could explain the Hall behaviour in these $BSCO_{2201}$ measurements. The first is the proximity of the van-Hove singularity, the second is an anisotropic scattering rate. The evidence for anisotropy could be explained in the former case by an anisotropy in the saddle point flat regions of the bandstructure, in the latter case the explanation is anisotropy in the scattering rate.

Assuming the latter, some interesting constraints are established for the scattering processes affecting in the Hall coefficient as follows,

1. Preferentially affects the electron or the hole portions of the Fermi surface

2. If it primarily affects the hole portions (along the $k = (\pi, \pi)$ vector), then the temperature dependence of the scattering weakens with doping

3. If it primarily affects the electron portions (along the $k = (\pi, 0)$ vector), then the temperature dependence of the scattering strengthens with doping

4. The scattering process is dominant below the temperature at which $R_H(\text{max})$ occurs, hardly affecting the data above this temperature

5. The scattering process appears linear in temperature

A natural continuation of this work would include a more precise determination of the low field region to determine with more certainty if the low temperature behaviour is truly T-linear as this would support the notion of an anisotropic parameter. A second possible experiment would be to measure the low temperature Hall in a material where the van-Hove does not have a significant momentum dependence in order to determine if the low temperature R_H continued to decay down to a level less than the room temperature term.

See Comments over.

There are not a lot of results or indeed conclusions ~~to~~. in this section. In particular I could not follow your reasoning on your determination of doping and in any case you have not explained why this is important to know. Perhaps the most interesting results are the T dep hall coefficient data. However you have not explained why the Hall coefficient is even T dependent in cuprates. Is this anomalous? ~~to~~ What theories have been put forward to explain it? Many people believe it results from Fermi surface reconstruction caused by stripe order or an ODW transition. There is no ~~[illegible]~~ significant discussion of this or ~~[illegible]~~ whether your data support this or not. The conclusions lack sufficient depth.